

Atom interferometer in a double-well potential

Karol Gietka and Jan Chwedeńczuk

Faculty of Physics, University of Warsaw, ul. Pasteura 5, 02-093 Warsaw, Poland

(Received 8 July 2014; published 1 December 2014)

We present a detailed study of an atom interferometer which can be realized in a double-well potential. We assume that the interferometric phase is imprinted in the presence of coherent tunneling between the wells. We calculate the ultimate bounds for the estimation sensitivity and show how they relate to the precision of the Mach-Zehnder interferometer. The interferometer presented here allows for sub-shot-noise sensitivity when fed with spin-squeezed states with either a reduced relative population imbalance or a reduced relative phase. We also calculate the precision of the estimation from the population imbalance and show that it overcomes the shot-noise limit when the entangled squeezed states are used at the input.

DOI: [10.1103/PhysRevA.90.063601](https://doi.org/10.1103/PhysRevA.90.063601)

PACS number(s): 37.25.+k, 03.75.Lm

I. INTRODUCTION

The key objective of quantum interferometry is to enhance the estimation precision $\Delta\theta$ of an unknown parameter θ using nonclassical correlations as a resource. The reference value $\Delta\theta_{\text{SN}} = \frac{1}{\sqrt{m}} \frac{1}{\sqrt{h_0^2 N}}$ is called the shot-noise limit (SNL). In this expression, N is the number of particles passing through the interferometer, m is the number of measurement repetitions, and h_0 characterizes the interferometric transformation. The SNL is the best achievable sensitivity in the classical two-mode interferometry. Only in the presence of useful particle entanglement can the SNL be surpassed [1,2] to give $\Delta\theta < \Delta\theta_{\text{SN}}$. Therefore, quantum interferometry can be viewed from two perspectives. From one point of view, the stress is put on the preparation of a usefully entangled quantum state which, together with the estimation protocol, gives $\Delta\theta < \Delta\theta_{\text{SN}}$. From the other point of view, interferometry is a tool for detecting quantum correlations in many-body systems. In this case, the value of $\Delta\theta$ is treated as a probe of the particle entanglement.

The sensitivity $\Delta\theta$ can be evaluated using the Cramér-Rao lower bound (CRLB) [3]. This important theorem links the sensitivity with the Fisher information:

$$\Delta\theta \geq \frac{1}{\sqrt{m}} \frac{1}{\sqrt{F}}. \quad (1)$$

The value of F depends on all three steps of the interferometric sequence: the preparation of the state which enters the device, the type of interferometric transformation, and the measurement performed at the output to obtain θ . According to the definition of the SNL, $F > h_0^2 N$ signals the particle entanglement [2]. However, in most experimental situations it is difficult to directly measure the value of F . The solution to this problem is to replace the Fisher information in Eq. (1) with some other physical quantity which is more accessible in the laboratory. However, this new quantity sets a weaker constraint than the CRLB (1).

This approach is illustrated by the broad use of the spin-squeezing parameter ξ_n^2 [4,5]. It is proportional to the fluctuations of the number of particles between the two modes divided by the visibility of the one-body fringes. Spin-squeezed states ($\xi_n^2 < 1$), which can be prepared in interacting systems of ultracold atoms [2,4–9], are particle entangled and potentially useful for quantum metrology. Recently, spin squeezing has been generated in two-mode quantum systems [7,8,10–14].

A similar technique to detect the nonclassical correlations was used in a collection of atoms scattered from a single Bose-Einstein condensate in spin-changing collisions [15].

A usefully entangled quantum state passes through a metrological device, for example, the Mach-Zehnder interferometer (MZI), which is realized in three steps. First, the two-mode state goes through a beam splitter, then the phase θ is imprinted on one of the arms, and finally another beam splitter mixes the modes to yield an interferometric signal. The MZI can benefit from quantum correlations present in the spin-squeezed state to provide the sensitivity $\Delta\theta$ below the SNL [2,16].

Another type of interferometric sequence is based on the Bloch oscillations of a gas in a double- or many-well trap [17–24]. In this scenario, the external force drives coherent oscillations between the sites of the periodic potential. Therefore, in contrast to the MZI, the mode mixing occurs simultaneously with the phase imprint. Such an interferometric protocol operating on spatially separated modes should be easier to handle in the experiment as compared to the MZI. This is because a beam splitter—which is a standard optical device—is difficult to implement with atoms. One approach is to trap the gas in two wells of a double-well potential, which represent the arms of an interferometer. The beam splitter is then realized by letting the gas tunnel between the wells for a given amount of time. This however requires precise control of the trapping potential. Another method was presented in Ref. [14], where the modes were mixed by spatially overlapping and then separating the two wells. Although state-of-the-art techniques were used, some motional excitations inevitably appeared in the system. Therefore, interferometric proposals which circumvent the direct implementation of a beam splitter might be relevant from the practical point of view. In this line, we study an interferometer where the phase imprint is accompanied by the tunneling of the gas between the two sites of the trapping potential. We demonstrate that such an interferometer does not overperform the MZI. Nevertheless, it might be easier to implement since no separate beam splitters are required.

This paper is organized as follows. In Sec. II, we introduce a simple model for the two-mode system of ultracold bosons trapped in a double-well potential. We determine the evolution operator and present the family of input states convenient for our analysis. In Sec. III, using the notion of the quantum Fisher information, we calculate the ultimate bounds for the

precision of such a double-well interferometer. In Sec. IV, we calculate the precision for a particular choice of estimation protocol and compare these results to the ultimate bounds. The conclusions are contained in Sec. V. This work is an extension of a previous study [25] where the outline of the theory of such an interferometer was presented.

II. THE MODEL

We consider a collection of N noninteracting bosons trapped in the symmetric double-well potential $V_{\text{dw}}(x)$. The system is driven into the oscillations between the two wells due to the presence of an external force with the potential $V(x)$. The objective of the following inquiry is to examine how and with what precision the strength of $V(x)$ can be determined. To accomplish this task, we employ the two-mode approximation where the field operator reads

$$\hat{\Psi}(x) = \psi_a(x)\hat{a} + \psi_b(x)\hat{b}. \quad (2)$$

Here, \hat{a} or \hat{b} annihilates a boson in a left or right potential well, and $\psi_a(x)$ or $\psi_b(x)$ is a corresponding spatial wave packet. The Hamiltonian of the system is

$$\hat{H} = \int dx \hat{\Psi}^\dagger(x) \left[-\frac{\hbar^2}{2M} \frac{\partial^2}{\partial x^2} + V_{\text{dw}}(x) + V(x) \right] \hat{\Psi}(x), \quad (3)$$

where M is the atomic mass. We employ the definition of the Josephson energy E_J and the detuning δ , i.e.,

$$E_J = 2 \int dx \psi_a^*(x) \left[-\frac{\hbar^2}{2M} \frac{\partial^2}{\partial x^2} + V_{\text{dw}}(x) \right] \psi_b(x), \quad (4a)$$

$$\delta = \int dx (|\psi_a(x)|^2 - |\psi_b(x)|^2) V(x), \quad (4b)$$

to obtain that, up to the constant terms, the Hamiltonian (3) can be expressed in a compact form:

$$\hat{H} = -E_J \hat{J}_x + \delta \hat{J}_z. \quad (5)$$

The \hat{J}_x and \hat{J}_z angular momentum operators which appear above, together with the y component, read

$$\hat{J}_x = \frac{1}{2}(\hat{a}^\dagger \hat{b} + \hat{b}^\dagger \hat{a}), \quad (6a)$$

$$\hat{J}_y = \frac{1}{2i}(\hat{a}^\dagger \hat{b} - \hat{b}^\dagger \hat{a}), \quad (6b)$$

$$\hat{J}_z = \frac{1}{2}(\hat{a}^\dagger \hat{a} - \hat{b}^\dagger \hat{b}). \quad (6c)$$

These operators form the Lie algebra $[\hat{J}_k, \hat{J}_l] = i\epsilon_{klm}\hat{J}_m$. The Hamiltonian (5) generates the unitary evolution

$$\hat{U} = \exp[i\varphi(\hat{J}_x - \epsilon \hat{J}_z)]. \quad (7)$$

Here $\epsilon = \delta/E_J$ is the ratio of the detuning to the Josephson energy, while $\varphi = E_J t/\hbar$ is the phase acquired through bare Josephson oscillations.

To simplify the further analysis, we assume that the initial state which undergoes the evolution (7) is pure:

$$|\psi\rangle = \sum_{n=0}^N C_n |n, N-n\rangle, \quad \text{with} \quad \sum_{n=0}^N |C_n|^2 = 1. \quad (8)$$

Depending on the coefficients C_n , $|\psi\rangle$ is either separable or entangled. Since this initial state is prepared in the absence of the perturbing potential $V(x)$, it is reasonable to assume that the state is path symmetric, i.e., $C_n = C_{N-n}$. This symmetry vastly simplifies the following discussion through the set of algebraic relations

$$\langle \hat{J}_y \rangle = \langle \hat{J}_z \rangle = \langle \hat{J}_x \hat{J}_y \rangle = \langle \hat{J}_x \hat{J}_z \rangle = \langle \hat{J}_y \hat{J}_z \rangle = 0. \quad (9)$$

The Hamiltonian (5) leads to various types of interferometric schemes depending on the ratio of the Josephson energy to the detuning δ . One limiting case is when the tunneling is fully suppressed during the action of the external force, i.e., $\epsilon \rightarrow \infty$. In such a case, the interferometric transformation consists of a bare phase imprint because the evolution operator (7) simplifies to

$$\hat{U}_{\text{ph}} = e^{-i\theta \hat{J}_z}, \quad (10)$$

where $\theta = \delta t/\hbar$. To obtain some θ -dependent signal, additional mode-mixing manipulation is necessary. Usually, two distinct scenarios are considered to accomplish this task. In the first one, the phase imprint (10) is preceded and followed by a pair of beam splitters, and the full cycle is the MZI with an effective evolution operator:

$$\hat{U}_{\text{MZI}} = e^{-i\theta \hat{J}_y}. \quad (11)$$

Note that when the two modes represent atomic internal degrees of freedom, the beam splitters can be realized by applying a precisely crafted rf pulse [7,8,15]. However, when the modes are spatially separated, as in a double-well potential [14,26–29], the beam splitter is more difficult to implement. In an alternative scenario of obtaining the interferometric signal from the evolution (10), the gas is simply released from the trap. In the far-field regime, an interference pattern is formed and θ can be inferred from the measurements of positions of individual atoms [30], for instance, from a least-square fit of the one-body density to the acquired data. In such a case, the sub-shot-noise (SSN) sensitivity can be achieved with the phase-squeezed states [30,31]. However, to reach the Heisenberg limit, the knowledge of the full N -body correlations is necessary [32], which for large N is practically impossible.

As underlined in the Introduction, we analyze the interferometer performance when both the tunneling and the detuning compete at the same time. Formally, this means that $\epsilon \lesssim 1$ and the evolution operator is given by the full expression (7), rather than the simplified Eq. (10). This type of evolution has one clear advantage over the above scenario. Namely, the modes are mixed already during the interaction of the gas with the external field, and no addition to the interferometric sequence is necessary.

It is worth noting that the Hamiltonian (5) generates a rotation of the composite spin- $\frac{N}{2}$ vector on the Bloch sphere. For such a transformation, states which give high metrological precision are those which have reduced fluctuations in a direction orthogonal to the rotation [1]. For instance, if the interferometer rotates the state around the y axis—as in the MZI (11)—the useful entanglement is related to the spin squeezing in the z direction. It might seem that finding a usefully entangled state for the Hamiltonian (5) should

be easy—one should just squeeze the state in a direction orthogonal to the vector with the Cartesian coordinates $(-E_J, 0, \delta)$. However, the knowledge of the direction of this vector is equivalent to the knowledge of δ , which, actually, is the parameter to be estimated. Although some adaptive methods could be used to first roughly estimate δ and then prepare properly entangled states, we assume that δ remains completely unknown, and the input states are typical for the two-mode atom interferometry.

Finally, note that during the evolution governed by the Hamiltonian (5), the two-body interactions are absent. This can be achieved by tuning the scattering length using the Feshbach resonances [33,34]. Although our analysis assumes a complete lack of interactions, some residual two-body collisions might be present [19]. In a more realistic model, they should be included either perturbatively in an analytical calculation or numerically.

III. ULTIMATE PRECISION—QUANTUM FISHER INFORMATION

In the first step, we calculate the maximal attainable precision of the estimation of δ . With this result at hand, we will have a possibility to judge the efficiency of a simple estimation protocol. Note that usually an interferometer is characterized by its phase sensitivity $\Delta\theta$. Here we use $\Delta\delta$, which is the precision of the estimation of the sole parameter δ . The phase sensitivity can be retrieved through a multiplication of $\Delta\delta$ by t/\hbar , where t is the time span of the interferometric sequence.

The ultimate precision $\Delta\delta$, which is optimized over all estimation strategies, is determined by the quantum Fisher information (QFI) denoted by F_Q . Its value depends on the input state $|\psi\rangle$ and the Hamiltonian (5) which introduces δ dependence into the system. For pure states, the ultimate CRLB is [35]

$$\Delta\delta \geq \frac{1}{\sqrt{m}} \frac{1}{\sqrt{F_Q}} = \frac{1}{\sqrt{m}} \frac{1}{\sqrt{4\langle(\Delta\hat{h})^2\rangle}}. \quad (12)$$

The variance $\langle(\Delta\hat{h})^2\rangle = \langle\hat{h}^2\rangle - \langle\hat{h}\rangle^2$ is calculated for the initial state $|\psi\rangle$, and \hat{h} is an operator which generates the transformation

$$i\partial_\delta|\psi(\delta)\rangle = \hat{h}|\psi(\delta)\rangle. \quad (13)$$

Using $|\psi(\delta)\rangle = \hat{U}|\psi\rangle$, we obtain that \hat{h} is related to the evolution operator (7) by the expression

$$\hat{h} = i\frac{\partial\hat{U}}{\partial\delta}\hat{U}^\dagger. \quad (14)$$

Note that it is convenient to express the sensitivity (12) in units of δ , i.e., to replace \hat{h} with $\delta \cdot \hat{h}$. Calculation of the QFI using Eqs. (7), (12), and (14) is straightforward. The commutation relations of the angular momentum operators give the rescaled generator equal to

$$\hat{h} = h_x\hat{J}_x + h_y\hat{J}_y + h_z\hat{J}_z, \quad (15)$$

where the three coefficients h_x , h_y , and h_z read

$$h_x = \frac{\epsilon^2}{\epsilon^2 + 1} \left(\frac{\sin(\varphi\sqrt{\epsilon^2 + 1})}{\sqrt{\epsilon^2 + 1}} - \varphi \right), \quad (16a)$$

$$h_y = \frac{\epsilon}{\epsilon^2 + 1} [1 - \cos(\varphi\sqrt{\epsilon^2 + 1})], \quad (16b)$$

$$h_z = \frac{\epsilon^3}{\epsilon^2 + 1} \left(\frac{\sin(\varphi\sqrt{\epsilon^2 + 1})}{\epsilon^2\sqrt{\epsilon^2 + 1}} + \varphi \right). \quad (16c)$$

Substituting Eq. (15) into Eq. (12), we obtain the following for the path-symmetric states (9):

$$F_Q = 4(h_x^2\langle(\Delta\hat{J}_x)^2\rangle + h_y^2\langle\hat{J}_y^2\rangle + h_z^2\langle\hat{J}_z^2\rangle). \quad (17)$$

Clearly, the QFI is a complicated function of the independent parameters ϵ and φ and of the input state (8) by means of the two lowest moments of the angular momentum operators.

We perform the systematic analysis of Eq. (17) by first fixing the input state—i.e., fixing $\langle(\Delta\hat{J}_x)^2\rangle$, $\langle\hat{J}_y^2\rangle$, and $\langle\hat{J}_z^2\rangle$ —and then plotting the QFI as a function of the other parameters.

We begin by establishing the SNL for the interferometric generator \hat{h} . The SNL is defined as the ultimate precision achievable by particle-separable states. For the interferometric transformation (15) the SNL can be evaluated using the spin-coherent state

$$|\psi\rangle = \frac{1}{\sqrt{N!}} \left(\frac{\hat{a}^\dagger + \hat{b}^\dagger}{\sqrt{2}} \right)^N |0\rangle, \quad (18)$$

which gives $\langle(\Delta\hat{J}_x)^2\rangle = 0$ and $\langle\hat{J}_y^2\rangle = \langle\hat{J}_z^2\rangle = \frac{N}{4}$. In such a case, the QFI scales linearly with the number of particles, and the SNL for our scheme is defined as

$$\frac{\Delta\delta}{\delta} \geq \frac{1}{\sqrt{m}} \frac{1}{\sqrt{N}} \frac{1}{\sqrt{h_y^2 + h_z^2}}. \quad (19)$$

From now on, we refer to the above expression as the correct SNL. Note, however, that for other interferometric transformations the value of the SNL might differ. For instance, the MZI interferometer gives the limiting value equal to

$$\frac{\Delta\delta_{\text{MZI}}}{\delta} \geq \frac{1}{\sqrt{m}} \frac{1}{\sqrt{N}} \frac{1}{\theta}. \quad (20)$$

Although in both cases the shot-noise scaling with the number of atoms is the same, Eqs. (19) and (20) have different coefficients. This is the price one pays for simultaneous mode mixing and phase imprint.

We now plot Eq. (19) in Fig. 1 as a function of φ for three different values of ϵ , in units of \sqrt{m} (i.e., the normalized sensitivity). For small $\epsilon = 0.25$, when the tunneling dominates over the detuning, oscillations are clearly visible. When ϵ grows, the period of the oscillations drops according to Eq. (16), and the sensitivity clearly improves with time. This is the result of the increasing domination of the $\delta\hat{J}_z$ term in the Hamiltonian (5). The fact that the sensitivity improves for large ϵ , as can be seen in Fig. 1, means that the interferometer performs at its best when the disturbance δ is large. On the other hand, when $\epsilon < 1$, which is of higher physical importance, we observe that the sensitivity reaches values of the order of 1. This means that the uncertainty of the estimation is

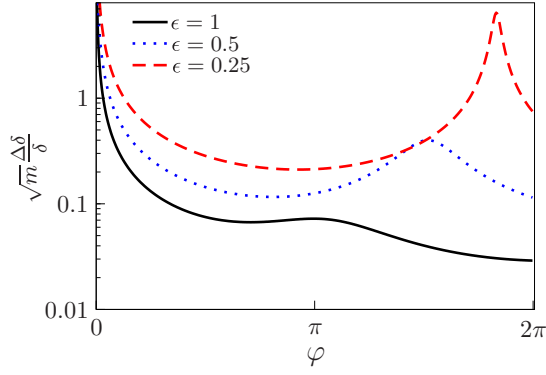


FIG. 1. (Color online) The normalized sensitivity $\Delta\delta$ in units of δ for a spin-coherent state with $N = 100$ plotted as a function of φ for three different values: $\epsilon = 1$ (solid black line), $\epsilon = 0.5$ (dotted blue line), and $\epsilon = 0.25$ (dashed red line).

comparable to the value of the parameter δ . Even in such a case, the estimation can be precise since for a large number of experiments m , according to the central limit theorem, the precision improves by a factor of $1/\sqrt{m}$.

In the next step, we replace the spin-coherent state with a spin-squeezed state which has reduced fluctuations of the relative atom number between the two modes [7,8,10–14]. Such a state is characterized with the spin-squeezing parameter [4,5]

$$\xi_n^2 = N \frac{\langle \hat{J}_z^2 \rangle}{\langle \hat{J}_x \rangle^2}. \quad (21)$$

We numerically generate an entangled spin-squeezed state by finding the ground state of the Bose-Hubbard Hamiltonian

$$\hat{H}_{\text{bh}} = -\hat{J}_x + \frac{\alpha}{N} \hat{J}_z^2, \quad (22)$$

with $N = 100$ particles and $\alpha > 0$. We take such an α to obtain a realistic value $\xi_n^2 = 0.15$. With this state, we calculate all the moments of the angular momentum operators (17) which determine the sensitivity (12). In Fig. 2, we plot the resulting normalized sensitivity in units of δ as a function of φ for the same three values of ϵ as in Fig. 1.

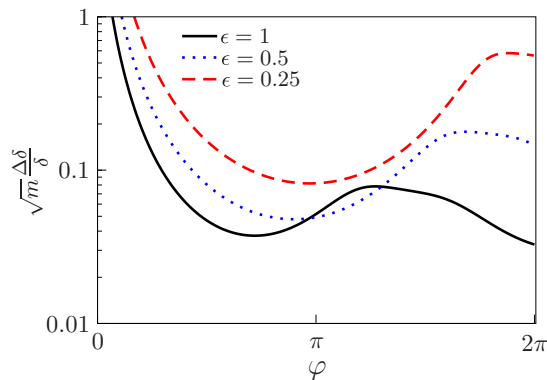


FIG. 2. (Color online) The normalized sensitivity $\Delta\delta$ in units of δ for a spin-squeezed state of $N = 100$ particles with $\xi_n^2 = 0.15$ plotted as a function of φ for three different values: $\epsilon = 1$ (solid black line), $\epsilon = 0.5$ (dotted blue line), and $\epsilon = 0.25$ (dashed red line).

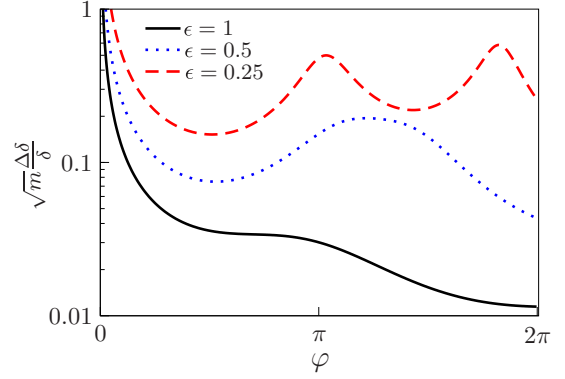


FIG. 3. (Color online) The normalized sensitivity $\Delta\delta$ in units of δ for a spin-squeezed state of $N = 100$ particles with $\xi_\phi^2 = 0.15$ plotted as a function of φ for three different values: $\epsilon = 1$ (solid black line), $\epsilon = 0.5$ (dotted blue line), and $\epsilon = 0.25$ (dashed red line).

Finally, we take a phase-squeezed state, characterized by the following squeezing parameter [30,31],

$$\xi_\phi^2 = N \frac{\langle \hat{J}_y^2 \rangle}{\langle \hat{J}_x \rangle^2}, \quad (23)$$

which we generate with the same Hamiltonian but with $\alpha < 0$. We take symmetrically $\xi_\phi^2 = 0.15$ for $N = 100$ particles and plot the analogical normalized sensitivity in Fig. 3.

We now discuss and compare the results presented in these three figures. First, note that, for large ϵ , phase-squeezed states ($\xi_\phi^2 < 1$) give better precision than number-squeezed states ($\xi_n^2 < 1$). This is because in this regime the $\delta \hat{J}_z$ term dominates in the Hamiltonian (5). For phase-squeezed states, the $\langle \hat{J}_z^2 \rangle$ term in the QFI dominates over the other two parts, and the coefficient h_z grows with ϵ . On the other hand, for number-squeezed states, the $\langle \hat{J}_y^2 \rangle$ term dominates over the other parts of the QFI. Moreover, according to Eqs. (16), this term becomes more important for small ϵ , but we still do not observe a significant improvement of the sensitivity between the results for the coherent state from Fig. 1 and the number-squeezed state from Fig. 2. To explain this behavior, we expand the coefficients (16) in the limit of $\epsilon \ll 1$ and short times ($\varphi \simeq 1$), and we obtain that

$$h_x \simeq \epsilon^2 (\sin \varphi - \varphi), \quad (24a)$$

$$h_y \simeq \epsilon (1 - \cos \varphi), \quad (24b)$$

$$h_z \simeq \epsilon \sin \varphi. \quad (24c)$$

Apart from the vicinity of $\varphi = 2\pi$, the h_x coefficient from Eq. (24a) can be neglected compared to h_y and h_z , and the lower bound for the sensitivity reads

$$\frac{\Delta\delta}{\delta} \geq \frac{1}{\sqrt{m}} \frac{1}{2\epsilon} \frac{1}{\sqrt{(1 - \cos \varphi)^2 \langle \hat{J}_y^2 \rangle + \sin^2 \varphi \langle \hat{J}_z^2 \rangle}}. \quad (25)$$

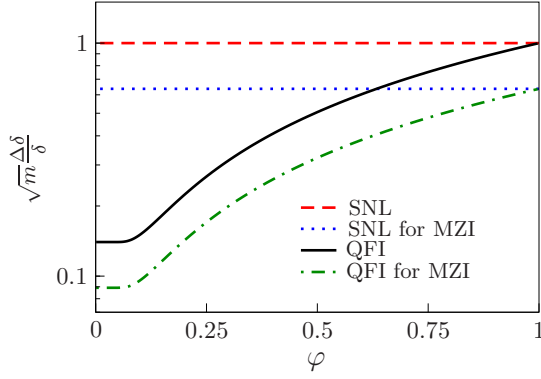


FIG. 4. (Color online) The QFI (solid black line) in units of SNL from Eq. (26) for $\epsilon = 0.1$ as a function of ξ_N . For a coherent state ($\xi_N = 1$) the sensitivity reaches the SNL (dashed red line). When $\xi_N < 1$, the sensitivity improves and breaks the SNL of the MZI (blue dashed line). For comparison, the sensitivity of the MZI, given by Eq. (27), is drawn with a green dot-dashed line.

Clearly, there is a particular point, $\varphi = \pi$, when

$$\frac{\Delta\delta}{\delta} \geq \frac{1}{\sqrt{m}} \frac{1}{2\epsilon} \frac{1}{\sqrt{4\langle \hat{J}_y^2 \rangle}}. \quad (26)$$

This sensitivity closely resembles the ultimate bound for the MZI interferometer (11), which for pure states reads

$$\frac{\Delta\delta_{\text{MZI}}}{\delta} \geq \frac{1}{\sqrt{m}} \frac{1}{\theta} \frac{1}{\sqrt{4\langle \hat{J}_y^2 \rangle}}. \quad (27)$$

However, since $\theta = \epsilon \times \varphi$, the MZI bound for the sensitivity is $\varphi/2$ times better than that of Eq. (26), as shown in Fig. 4.

This means that the precision (27), in contrast to Eq. (26), improves over time. Nevertheless, since the expansion (24) is valid for short times, the gain from the time scaling of Eq. (27) over Eq. (26) is of the order of π . Note also that Eq. (26) improves for the spin-squeezed states with $\xi_n^2 < 1$ because for such states $4\langle \hat{J}_y^2 \rangle > N$, but, on the other hand, it deteriorates when ϵ drops. These two effects more or less cancel each other for the parameters used in Fig. 2. However, for large N , the improvement coming from the quantum correlations dominates over the loss of the signal, leading to the SSN scaling of the sensitivity.

Another distinguished time is when $\phi = \frac{\pi}{2}$. Then, Eq. (25) simplifies to

$$\frac{\Delta\delta}{\delta} \geq \frac{1}{\sqrt{m}} \frac{1}{\epsilon} \frac{1}{\sqrt{4\langle \hat{J}_y^2 \rangle + 4\langle \hat{J}_z^2 \rangle}}. \quad (28)$$

Interestingly, in this case the sensitivity can be improved over the SNL for both phase-squeezed states, which give $4\langle \hat{J}_z^2 \rangle > N$, or number-squeezed states, which give $4\langle \hat{J}_y^2 \rangle > N$. Still, the loss of the signal for small ϵ , in comparison to the sensitivity of the MZI (27), can overshadow the SSN scaling if N is not sufficiently large.

Finally, we focus on the long-time behavior of the QFI. When $\varphi \gg 1$, Eqs. (16) simplify and give the following bound

for the sensitivity:

$$\frac{\Delta\delta}{\delta} \geq \frac{1}{\sqrt{m}} \frac{\epsilon^2 + 1}{\theta\epsilon} \frac{1}{\sqrt{4\langle (\Delta\hat{J}_x)^2 \rangle + 4\langle \hat{J}_z^2 \rangle \epsilon^2}}. \quad (29)$$

If $\epsilon \ll 1$ and the state is spin squeezed with $\xi_n^2 < 1$, the $4\langle \hat{J}_z^2 \rangle \epsilon^2$ term can be safely neglected, and we obtain

$$\frac{\Delta\delta}{\delta} \geq \frac{1}{\sqrt{m}} \frac{1}{\theta\epsilon} \frac{1}{\sqrt{4\langle (\Delta\hat{J}_x)^2 \rangle}}. \quad (30)$$

If $|\psi\rangle$ is strongly squeezed—i.e., it is close to the twin-Fock state $|\psi\rangle \simeq |\frac{N}{2}, \frac{N}{2}\rangle$ —then $\langle (\Delta\hat{J}_x)^2 \rangle \simeq \langle \hat{J}_y^2 \rangle$, and Eqs. (27) and (30) differ only by a presence of ϵ in the denominator of the latter. Still, both expressions share the same scaling of the sensitivity with time. When $\epsilon \simeq 1$ and $|\psi\rangle$ is close to a coherent spin state or is phase squeezed, then Eq. (29) is approximately

$$\frac{\Delta\delta}{\delta} \geq \frac{1}{\sqrt{m}} \frac{\epsilon^2 + 1}{\theta\epsilon^2} \frac{1}{\sqrt{4\langle \hat{J}_z^2 \rangle}}. \quad (31)$$

This expression gives the SSN scaling for phase-squeezed states, scales inversely in time, and is only $\frac{\epsilon^2 + 1}{\epsilon^2} \simeq 2$ times worse than the ultimate bound for the pure phase imprint (10).

To summarize this section, we have calculated the ultimate bound for the sensitivity of the double-well interferometer. We have shown that it betrays the characteristic oscillatory behavior due to the presence of the Josephson term in the Hamiltonian (5). We have also shown that for some particular instants of time, the QFI can be improved beyond the SNL with either number-squeezed or phase-squeezed states. At long times and with spin-squeezed input states with the reduced relative population imbalance ($\xi_n^2 < 1$), the sensitivity closely resembles that of the MZI, whereas with phase-squeezed states ($\xi_\phi^2 < 1$), it is almost as good as for a pure phase imprint.

IV. ESTIMATION FROM THE POPULATION IMBALANCE

We now focus on a particular scheme of estimation based on the measurement of the population imbalance. The sequence we consider is the following. First, the input state (8) evolves according to Eq. (7). Next, a population imbalance n between the two sites is measured. If these data are used to estimate the value of δ , the CRLB reads

$$\Delta\delta \geq \frac{1}{\sqrt{m}} \frac{1}{\sqrt{F_{\text{imb}}}}. \quad (32)$$

Here, F_{imb} is the Fisher information for the population imbalance measurement. It is related to the conditional probability $p(n|\delta)$ for detecting n given δ as follows:

$$F_{\text{imb}} = \sum_{n=0}^N \frac{1}{p(n|\delta)} \left(\frac{\partial p(n|\delta)}{\partial \delta} \right)^2. \quad (33)$$

The above probability results from the projection of the output state onto a state with n particles in one mode and $N - n$ in the other:

$$p(n|\delta) = |\langle n, N - n | \hat{U} | \psi \rangle|^2. \quad (34)$$

The Fisher information (33) through the CRLB (32) provides the maximal precision for the estimation of δ from the population imbalance measurement, whichever estimator is used. Moreover, $F_Q \geq F_{\text{imb}}$ always holds since the QFI sets the ultimate CRLB optimized over all possible measurements.

Although the Fisher information from Eq. (33) is “the best one can get” from the population imbalance measurement, reaching the bound (32) requires the knowledge of the full probability (34). This renders the Fisher information approach impractical in most of the cases because in order to know Eq. (34) one must go through a laborious calibration stage. Therefore, typically some simpler estimators, which still utilize the data acquired from the measurements of the population imbalance, are used. The simplest estimator is based on the knowledge of the lowest moment of Eq. (34), namely, the average, which is equal to the mean of the population imbalance operator \hat{J}_z :

$$\langle n(t) \rangle = \sum_{n=-\frac{N}{2}}^{\frac{N}{2}} \left(n - \frac{N}{2} \right) p(n|\delta) = \langle \hat{J}_z(t) \rangle. \quad (35)$$

This average can be evaluated in the Heisenberg picture, where \hat{J}_z reads

$$\hat{J}_z(t) = \hat{U}^\dagger \hat{J}_z \hat{U}. \quad (36)$$

Using the evolution operator (7), we obtain

$$\hat{J}_z(t) = u_x(t)\hat{J}_x + u_y(t)\hat{J}_y + u_z(t)\hat{J}_z. \quad (37)$$

The three time-dependent coefficients are

$$u_x(t) = \frac{\epsilon[\cos(\varphi\sqrt{\epsilon^2+1}) - 1]}{\epsilon^2+1}, \quad (38a)$$

$$u_y(t) = -\frac{\sin(\varphi\sqrt{\epsilon^2+1})}{\sqrt{\epsilon^2+1}}, \quad (38b)$$

$$u_z(t) = \frac{\cos(\varphi\sqrt{\epsilon^2+1}) + \epsilon^2}{\epsilon^2+1}. \quad (38c)$$

The scheme of the estimation from the average population imbalance is presented in Refs. [25,30,32]. First, we assume that the function (35) is known with δ being a free parameter. In the experiment, this function is obtained in the calibration process. Then, the population imbalance is measured m times at time t . According to the central limit theorem, if $m \gg 1$, the averaged outcomes are distributed with a Gaussian probability around the true mean value. This probability, together with the experimental outcomes, is used to construct the likelihood function $\mathcal{L}(\delta)$. In the final step, δ is assigned to the value maximizing $\mathcal{L}(\delta)$. Such an estimator is unbiased, and its sensitivity is given by the error-propagation formula

$$\Delta\delta \geq \frac{1}{\sqrt{m}} \frac{\sqrt{\langle [\Delta\hat{J}_z(t)]^2 \rangle}}{\left| \frac{\partial \langle \hat{J}_z(t) \rangle}{\partial \delta} \right|}. \quad (39)$$

The average and the variance of the population imbalance operator are expressed in terms of the two lowest moments of the angular momentum operators and the coefficients u_i . Combining Eqs. (37), (38), and (39), we obtain the bound for

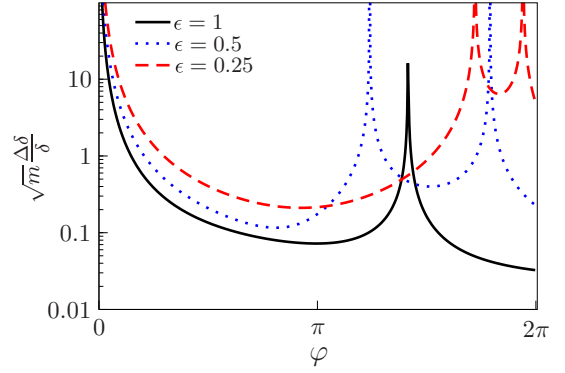


FIG. 5. (Color online) The normalized sensitivity $\Delta\delta$ in units of δ calculated using the error propagation formula for a spin-coherent state with $N = 100$. The figure shows Eq. (41) as a function of φ for three different values: $\epsilon = 1$ (solid black line), $\epsilon = 0.5$ (dotted blue line), and $\epsilon = 0.25$ (dashed red line).

the sensitivity in units of δ :

$$\frac{\Delta\delta}{\delta} \geq \frac{1}{\sqrt{m}} \frac{\sqrt{u_x^2(t)N \frac{\langle (\Delta\hat{J}_x)^2 \rangle}{\langle \hat{J}_x \rangle^2} + u_y^2(t)\xi_\phi^2 + u_z^2(t)\xi_n^2}}{\sqrt{N}\delta \left| \frac{\partial u_x(t)}{\partial \delta} \right|}. \quad (40)$$

It is again a complicated function of ϵ , φ , and the input state. For a particular case of a spin-coherent state (18), when $\xi_n^2 = \xi_\phi^2 = 1$, we obtain that

$$\frac{\Delta\delta}{\delta} \geq \frac{1}{\sqrt{m}} \frac{\sqrt{u_y^2(t) + u_z^2(t)}}{\sqrt{N}\delta \left| \frac{\partial u_x(t)}{\partial \delta} \right|}. \quad (41)$$

We plot this result in Fig. 5 as a function of φ for the same three values of ϵ as in Fig. 1. We observe behavior similar to that in the case of the ultimate bound discussed in Sec. III. For each ϵ , the sensitivity reveals some oscillatory features, and the values of $\Delta\delta/\delta$ are similar to those in Fig. 1. To complete the comparison, in Figs. 6 and 7, we plot Eq. (40) for the number-squeezed state ($\xi_n^2 = 0.15$) and the phase-squeezed state ($\xi_\phi^2 = 0.15$). Again, we observe the typical oscillatory behavior and quite similar values of the sensitivity.

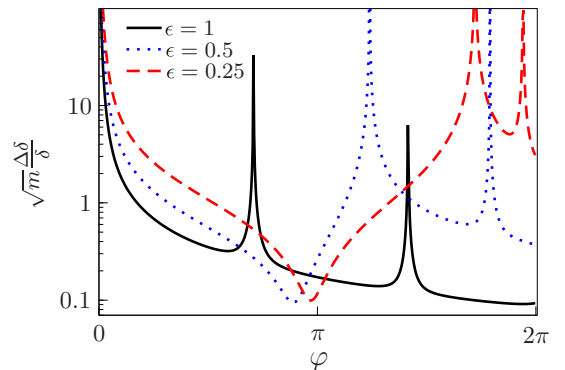


FIG. 6. (Color online) The normalized sensitivity in units of δ calculated using the error propagation formula for a number-squeezed state of $N = 100$ particles with $\xi_n^2 = 0.15$. The figure shows Eq. (40) as a function of φ for three different values: $\epsilon = 1$ (solid black line), $\epsilon = 0.5$ (dotted blue line), and $\epsilon = 0.25$ (dashed red line).

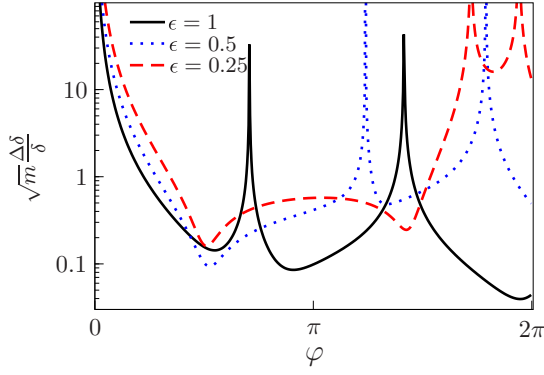


FIG. 7. (Color online) The normalized sensitivity $\Delta\delta$ in units of δ calculated using the error propagation formula for a phase-squeezed state of $N = 100$ particles with $\xi_\phi^2 = 0.15$. The figure shows Eq. (40) as a function of φ for three different values: $\epsilon = 1$ (solid black line), $\epsilon = 0.5$ (dotted blue line), and $\epsilon = 0.25$ (dashed red line).

In order to gain a better insight into the precision that can be achieved from Eq. (40), we again consider the $\epsilon \ll 1$ and $\varphi \simeq 1$ case. In this limit, we obtain that

$$\frac{\Delta\delta}{\delta} \geq \frac{1}{\sqrt{m}} \frac{1}{\sqrt{N}} \frac{1}{\epsilon} \frac{\sqrt{\xi_\phi^2 \sin^2 \varphi + \xi_n^2 \cos^2 \varphi}}{|\cos \varphi - 1|}. \quad (42)$$

To draw a parallel with the results from Sec. III, we first consider the case $\varphi = \pi$, which simplifies Eq. (42) to

$$\frac{\Delta\delta}{\delta} \geq \frac{1}{\sqrt{m}} \frac{1}{\sqrt{N}} \frac{1}{2\epsilon} \xi_n. \quad (43)$$

This expression resembles the sensitivity of the estimation from the average population imbalance with the MZI,

$$\frac{\Delta\delta_{\text{MZI}}}{\delta} \geq \frac{1}{\sqrt{m}} \frac{1}{\sqrt{N}} \frac{1}{\theta} \xi_n, \quad (44)$$

just as Eq. (26) resembles the ultimate bound of the MZI. Again, the ratio of those two is equal to $\varphi/2$. Nevertheless, the precision (43) improves below the SNL if the interferometer is fed with a squeezed state with $\xi_n^2 < 1$.

The other distinguished instant of time is when $\varphi = \frac{\pi}{2}$. At this point, Eq. (42) transforms into

$$\frac{\Delta\delta}{\delta} \geq \frac{1}{\sqrt{m}} \frac{1}{\sqrt{N}} \frac{1}{\epsilon} \xi_\phi. \quad (45)$$

Again, there is a close analogy between this expression and the bound from Eq. (28). As in the case of Eq. (28), the sensitivity (45) drops below the SNL if the input state is phase-squeezed ($\xi_\phi^2 < 1$). Note, however, that the presence of ϵ in the denominator deteriorates the precision.

At long times—when $\varphi \gg 1$ —and when ϵ is small, the formula (42) takes an appealing form:

$$\frac{\Delta\delta}{\delta} \geq \frac{1}{\sqrt{m}} \frac{1}{\sqrt{N}} \frac{1}{\theta\epsilon^2} \sqrt{\xi_\phi^2 + \xi_n^2 \cot^2 \varphi}. \quad (46)$$

Again, this expression scales inversely with time. At times such that $\cot^2 \varphi = 0$, this sensitivity, analogically to the short-time expression (45), improves over the shot-noise scaling with phase-squeezed states. Nevertheless, the improvement from

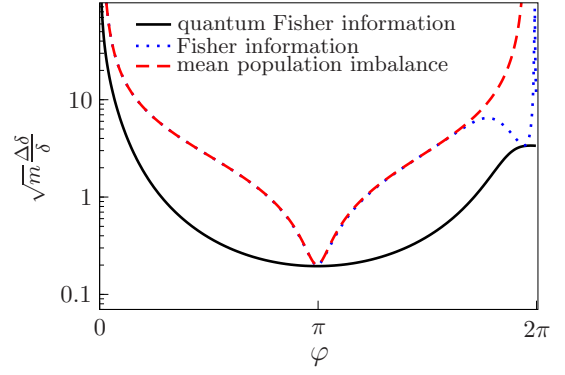


FIG. 8. (Color online) Comparison of the three bounds for the normalized estimation precision. The solid black line is the QFI from Eq. (12). The dotted blue line is obtained from the full population imbalance probability (34). The dashed red line is the error propagation formula for the estimation from the lowest moment of the population imbalance probability. The parameters are $\epsilon = 0.1$, $\xi_n^2 = 0.15$, and $N = 100$.

the particle entanglement might be eclipsed by the presence of ϵ^2 in the denominator.

Finally, we compare the ultimate sensitivity (12) to the Fisher information (32) and the error propagation formula (40). In Fig. 8, we plot the normalized ($\sqrt{m} \frac{\Delta\delta}{\delta}$) sensitivity in units of δ with $\epsilon = 0.1$ as a function of φ for a spin-squeezed state with $\xi_n^2 = 0.15$. We observe that the simple estimation from the average population imbalance gives the sensitivity almost as good as the Fisher information. Moreover, for $\varphi = \pi$ —when Eqs. (26) and (43) hold—all three methods give the same precision. This result can be explained as follows. At this time point, the sensitivities (26) and (43) resemble the precision of the MZI. For this interferometer, the Fisher information for the population imbalance probability (32) saturates the QFI for all states (8) with real coefficients C_n [36,37]. A spin-squeezed ground state of the Hamiltonian (22) satisfies this condition, therefore Eqs. (26) and (32) must coincide. On the other hand, such a state is Gaussian, meaning that it is characterized by the two lowest correlation functions. Not surprisingly, in such a case the sensitivity, which depends on these two moments (39), is as powerful as the estimation from the full probability (32). To summarize, at $\varphi = \pi$ the simple estimation protocol from the average population imbalance is optimal; i.e., it saturates the ultimate bound of the QFI.

V. CONCLUSIONS

We performed a systematic study of an atom interferometer which can be implemented in a double-well potential. This interferometer combines the phase imprint and the mode mixing at the same time. We derived the ultimate bounds for the precision of the parameter estimation and showed that these bounds improve from the particle entanglement of spin-squeezed states. Importantly, for such an interferometer the estimation from the average population imbalance gives the sensitivity which closely resembles the expression obtained for the MZI. Finally, we showed that this estimation method can be optimal at the half of the period of the Josephson oscillation. Such an oscillation-assisted interferometer,

similarly to the Mach-Zehnder interferometer, can benefit from the time scaling of the sensitivity. However, in every limiting case, the precision of the interferometer suffers from the loss of the signal, represented by the presence of ϵ in the denominator.

Our work shows that a simple evolution operator (7) allows for an astonishing variety of interferometric scenarios, though the presented analysis is not general. We restricted our calculations only to pure states and assumed that the interactions are fully suppressed during the interferometric sequence. In some situations, the interactions might either improve the interferometric signal [38] or barely affect it [39]. Nevertheless, in most cases the presence of interactions worsens the visibility of the interferometric fringes [10]. To

avoid such effects, the two-body collisions are tuned down to zero with the help of Feshbach resonances [17].

We also did not take into account the impact of decoherence [40–42]. In any realistic application, the above theory should be extended to include those effects. Nevertheless, our results serve for two purposes. First, the idealized model determines the ultimate bounds for the precision of the parameter estimation. Second, these findings provide a simple theoretical background for further analysis.

ACKNOWLEDGMENT

This work was supported by the National Science Center under Grant No. DEC-2011/03/D/ST2/00200.

-
- [1] V. Giovannetti, S. Lloyd, and L. Maccone, *Science* **306**, 1330 (2004).
- [2] L. Pezzé and A. Smerzi, *Phys. Rev. Lett.* **102**, 100401 (2009).
- [3] A. Holevo, *Probabilistic and Statistical Aspects of Quantum Theory* (Scuola Normale Superiore, Pisa, 2011).
- [4] M. Kitagawa and M. Ueda, *Phys. Rev. A* **47**, 5138 (1993).
- [5] D. J. Wineland, J. J. Bollinger, W. M. Itano, and D. J. Heinzen, *Phys. Rev. A* **50**, 67 (1994).
- [6] Y. P. Huang and M. G. Moore, *Phys. Rev. Lett.* **100**, 250406 (2008).
- [7] C. Gross, T. Zibold, E. Nicklas, J. Esteve, and M. K. Oberthaler, *Nature (London)* **464**, 1165 (2010).
- [8] M. F. Riedel, P. Böhi, Y. Li, T. W. Hänsch, A. Sinatra, and P. Treutlein, *Nature (London)* **464**, 1170 (2010).
- [9] H. Strobel, W. Muessel, D. Linnemann, T. Zibold, D. B. Hume, L. Pezzé, A. Smerzi, and M. K. Oberthaler, *Science* **345**, 424 (2014).
- [10] J. Esteve, C. Gross, A. Weller, S. Giovanazzi, and M. Oberthaler, *Nature (London)* **455**, 1216 (2008).
- [11] J. Appel, P. J. Windpassinger, D. Oblak, U. B. Hoff, N. Kjærgaard, and E. S. Polzik, *Proc. Natl. Acad. Sci. USA* **106**, 10960 (2009).
- [12] I. D. Leroux, M. H. Schleier-Smith, and V. Vuletić, *Phys. Rev. Lett.* **104**, 250801 (2010).
- [13] Z. Chen, J. G. Bohnet, S. R. Sankar, J. Dai, and J. K. Thompson, *Phys. Rev. Lett.* **106**, 133601 (2011).
- [14] T. Berrada, S. van Frank, R. Bücker, T. Schumm, J.-F. Schaff, and J. Schmiedmayer, *Nat. Commun.* **4**, 2077 (2013).
- [15] B. Lücke, M. Scherer, J. Kruse, L. Pezzé, F. Deuretzbacher, P. Hyllus, J. Peise, W. Ertmer, J. Arlt, L. Santos *et al.*, *Science* **334**, 773 (2011).
- [16] L. Pezzé and A. Smerzi, *Phys. Rev. A* **73**, 011801 (2006).
- [17] G. Ferrari, N. Poli, F. Sorrentino, and G. M. Tino, *Phys. Rev. Lett.* **97**, 060402 (2006).
- [18] N. Poli, F.-Y. Wang, M. G. Tarallo, A. Alberti, M. Prevedelli, and G. M. Tino, *Phys. Rev. Lett.* **106**, 038501 (2011).
- [19] M. Fattori, C. D’Errico, G. Roati, M. Zaccanti, M. Jona-Lasinio, M. Modugno, M. Inguscio, and G. Modugno, *Phys. Rev. Lett.* **100**, 080405 (2008).
- [20] P. Cladé, E. de Mirandes, M. Cadoret, S. Guellati-Khélifa, C. Schwob, F. Nez, L. Julien, and F. Biraben, *Phys. Rev. Lett.* **96**, 033001 (2006).
- [21] I. Carusotto, L. Pitaevskii, S. Stringari, G. Modugno, and M. Inguscio, *Phys. Rev. Lett.* **95**, 093202 (2005).
- [22] R. Battesti, P. Cladé, S. Guellati-Khélifa, C. Schwob, B. Grémaud, F. Nez, L. Julien, and F. Biraben, *Phys. Rev. Lett.* **92**, 253001 (2004).
- [23] M. Ben Dahan, E. Peik, J. Reichel, Y. Castin, and C. Salomon, *Phys. Rev. Lett.* **76**, 4508 (1996).
- [24] P. Cladé, *arXiv:1405.2770*.
- [25] J. Chwedeńczuk, L. Pezzé, F. Piazza, and A. Smerzi, *Phys. Rev. A* **82**, 032104 (2010).
- [26] R. Gati, B. Hemmerling, J. Fölling, M. Albiez, and M. K. Oberthaler, *Phys. Rev. Lett.* **96**, 130404 (2006).
- [27] G.-B. Jo, Y. Shin, S. Will, T. A. Pasquini, M. Saba, W. Ketterle, D. E. Pritchard, M. Vengalattore, and M. Prentiss, *Phys. Rev. Lett.* **98**, 030407 (2007).
- [28] T. Schumm, S. Hofferberth, L. M. Andersson, S. Wildermuth, S. Groth, I. Bar-Joseph, J. Schmiedmayer, and P. Krüger, *Nat. Phys.* **1**, 57 (2005).
- [29] P. Böhi, M. F. Riedel, J. Hoffrogge, J. Reichel, T. W. Hänsch, and P. Treutlein, *Nat. Phys.* **5**, 592 (2009).
- [30] J. Chwedeńczuk, P. Hyllus, F. Piazza, and A. Smerzi, *New J. Phys.* **14**, 093001 (2012).
- [31] J. Grond, U. Hohenester, I. Mazets, and J. Schmiedmayer, *New J. Phys.* **12**, 065036 (2010).
- [32] J. Chwedeńczuk, F. Piazza, and A. Smerzi, *New J. Phys.* **13**, 065023 (2011).
- [33] H. Feshbach, *Ann. Phys.* **5**, 357 (1958).
- [34] C. J. Pethick and H. Smith, *Bose-Einstein Condensation in Dilute Gases* (Cambridge University Press, Cambridge, UK, 2008).
- [35] S. L. Braunstein and C. M. Caves, *Phys. Rev. Lett.* **72**, 3439 (1994).
- [36] T. Wasak, J. Chwedeńczuk, L. Pezzé, and A. Smerzi, *arXiv:1310.2844*.
- [37] M. D. Lang and C. M. Caves, *Phys. Rev. Lett.* **111**, 173601 (2013).
- [38] I. Tikhonenkov, M. G. Moore, and A. Vardi, *Phys. Rev. A* **82**, 043624 (2010).
- [39] J. Grond, U. Hohenester, J. Schmiedmayer, and A. Smerzi, *Phys. Rev. A* **84**, 023619 (2011).
- [40] R. Demkowicz-Dobrzański, J. Kołodyński, and M. Guta, *Nat. Commun.* **3**, 1063 (2012).
- [41] A. W. Chin, S. F. Huelga, and M. B. Plenio, *Phys. Rev. Lett.* **109**, 233601 (2012).
- [42] P. Szankowski, J. Chwedeńczuk, and M. Trippenbach, *arXiv:1212.2528*.